npj Materials Degradation

https://doi.org/10.1038/s41529-026-00756-1

Article in Press

Toward the performance assessment of advanced nuclear waste forms: temperature dependence of lanthanide borosilicate glass dissolution

Received: 30 October 2025

Accepted: 3 February 2026

Cite this article as: McLachlan, J.R., Stanley, D.A., Garcia, J.A. *et al.* Toward the performance assessment of advanced nuclear waste forms: temperature dependence of lanthanide borosilicate glass dissolution. *npj Mater Degrad* (2026). https://doi.org/10.1038/s41529-026-00756-1

Jeffrey R. McLachlan, Dalton A. Stanley, Justine A. Garcia, Ta-Chun Wang, Leslie G. Castro, Ethan Bates, Stefan Finsterle, Jesse Sloane, Per F. Peterson, Raluca O. Scarlat & Rebecca J. Abergel

Toward the Performance Assessment of Advanced Nuclear Waste Forms: Temperature Dependence of Lanthanide Borosilicate Glass Dissolution

Jeffrey R. McLachlan[a,b]*, Dalton A. Stanley[a,c], Justine A. Garcia[c,d], Ta-Chun Wang[b], Leslie G. Castro[a,c], Ethan Bates[e], Stefan Finsterle[f], Jesse Sloane[g], Per F. Peterson[b], Raluca O. Scarlat[b], Rebecca J. Abergel[a,b,c]*

[a] Chemical Sciences Division, Lawrence Berkeley National Laboratory, Berkeley, California 94720, United States

[b] Department of Nuclear Engineering, University of California, Berkeley, California 94720, United States

[c] Department of Chemistry, University of California, Berkeley, California 94720, United States

[d] Department of Chemistry, California State University, Hayward, California 94542, United States

[e] Cambrian Nuclear, Inc. Union City, California 94587, United States

[f] Finsterle GeoConsulting, LLC, Kensington, California 94708, United States

[g] Deep Isolation Nuclear, Inc. Berkeley, California 94704, United States

*jmclachlan@berkeley.edu and abergel@berkeley.edu

Abstract

Lanthanide borosilicate (LaBS) glasses are among the most promising waste forms for the immobilization of high-level radioactive waste generated from advanced nuclear fuel cycles. However, the temperature dependence of their dissolution kinetics remains poorly understood and constrained, limiting the integration of these materials into established performance assessment models. Here, we investigate the dissolution behavior of the legacy AmCm2-19 LaBS glass and the benchmark alkali aluminoborosilicate ISG-1 in deionized water between 50 °C and 250 °C using ASTM C1285 (Product Consistency Test-B) protocols. For AmCm2-19 LaBS glass, normalized elemental release rates for boron and silicon increase with temperature before plateauing near 150 °C, consistent with solubility-limited behavior. From data obtained at 50 °C and 100 °C, Arrhenius analysis yields activation energies of E_a(B) = 24.8 ± 0.3 kJ mol^{-1} and E_a(Si) = 14.4 ± 0.2 kJ mol^{-1}, similar or slightly lower than those previously reported for two other compositions of LaBS glasses. No secondary phases or alteration layers were detected by SEM-EDX or pXRD. These results establish one of the first temperature-dependent kinetic datasets for LaBS glass dissolution, providing quantitative parameters to inform mechanistic corrosion models and predictive simulations of glass degradation in geological disposal environments.

Introduction

High-level radioactive waste (HLW), such as those generated from the operation of nuclear reactors or the reprocessing of spent nuclear fuels, must be managed appropriately to ensure the present and future safety of the population and environment. Presently, international organizations and several nuclear nations have recommended a defense-in-depth disposal strategy where multiple barrier systems are used to prevent the mobilization of radionuclides through the environment and into the biosphere.[1] This approach typically involves (1) the conversion of HLW into a durable waste form that resists dissolution in water, (2) placing the waste form into a sealed canister system that aids in its transportation and storage, and delays the waste form from contacting water upon disposal, and (3) emplacing the canister into a mined or borehole geological repository that has been selected and engineered to mitigate the transportation of radionuclides to the biosphere in appreciable quantities on the epoch timescale. Before a HLW disposal scheme can be approved, the safety of the entire proposed system must be assessed. This is often achieved through the implementation of a performance assessment model (PAM) that comprises an integrated set of sub-models that track the release of safety-relevant radionuclides from the waste form and through the environment as a function of time and many other intertwined parameters.[2] One sub-model of the PAM, denoted the source-term model, describes the rate at which radionuclides are released from the waste form due to contact with water, and accounts for changes in the ever-evolving parameters of the system such as pH, temperature, leachate composition, and more.[3,4] Thus, the effect these parameters have on the durability of a waste form must be understood to justify the implementation of the most detailed source-term model possible.[5]

Many waste forms have been proposed for the disposal of various types of HLW, including several glasses, ceramics, grouts, cements, minerals, composites, and the fuel forms themselves.[6] The selection of a waste form for a specified HLW-repository disposal scheme depends on factors such as safety, cost, technological readiness, and knowledge of the waste forms' durability in aqueous media similar to that of the designated repository. For HLW arising from the reprocessing of spent fuel generated from the operation of traditional water-cooled nuclear reactors, alkali aluminoborosilicate (AAB) glasses have been the most studied and broadly accepted waste form to date. Several review articles and government reports have been dedicated to summarizing the thousands of publications that explore the effect various system parameters, such as pH, temperature, glass composition, leachate composition, radiation, and glass surface area, have on the short-term and long-term durability of these materials in aqueous systems.[7–11] From these studies, detailed source-term models have been developed,[12–14] typically taking the form of:

$$r(t) = k_0 \cdot 10^{\eta \cdot (pH(t)-7)} \cdot e^{-\frac{E_a}{R \cdot T(t)}} \cdot \left(1 - \frac{Q(t)}{K_{sat}}\right) \cdot SA(t) \cdot \Upsilon \quad \textbf{(1)}$$

$$\Upsilon = \Upsilon_{rad} \cdot \Upsilon_{leachate} \cdot \Upsilon_{SA} \quad \textbf{(2)}$$

where $r(t)$ is the time-dependent rate of radionuclide release, k_0 is the forward rate of dissolution, η is the pH power law coefficient, E_a is the activation energy of the dissolution reaction, R is the ideal gas constant, K_{sat} is the effective equilibrium constant of the dissolution reaction, Υ is a dimensionless factor used to account for waste form fracturing (Υ_{SA}), radiation (Υ_{rad}), and leachate compositional effects ($\Upsilon_{leachate}$), and $pH(t)$, absolute temperature ($T(t)$), the reaction quotient of the dissolution reaction ($Q(t)$), and geometric surface area ($SA(t)$) are time-dependent parameters. Note that other more sophisticated models, such as the GRAAL model,[15–18] have been proposed but will not be discussed further in this work due to their minimal application to complex glass and leachate compositions to date. When insufficient or uncertain data is available to advise the selection of input parameters of the model, conservative simplifications are made. The source-term model for the disposal of HLW AAB glass at the United States Department of Energy (DOE) Yucca Mountain site utilized a simplified version of **Equation 1** that combined the affinity term ($1-Q(t)/K_{sat}$), Υ, and k_0 into a single constant term, denoted k_E, which was assigned a conservative range of values.[19,20] The Swiss Nationale Genossenschaft für die Lagerung radioaktiver Abfälle (NAGRA) utilized a simpler source-term model where waste form degradation rates are held constant through time, and a broad range of constant degradation rates are selected to bracket optimistic and pessimistic scenarios. In a recent report, they selected a range of degradation rates spanning 4 orders of magnitude to account for uncertainties in the long-term degradation behavior of SON68 type glasses in a Opalinus Clay geological formation.[21] These cases highlight the depth of knowledge required to confidently model the long-term durability of waste forms in geological repositories.

Several countries have pushed for the development and implementation of advanced reactors that may utilize fuel forms (i.e., metal alloy, metal oxide, tri-structural isotropic particle, and salt), neutron spectra (thermal vs. fast), and coolants (i.e., molten salt, molten metal, super critical water, and gas) that vastly differ from those used with traditional water-cooled nuclear reactors.[22,23] The operation of these advanced reactors will undoubtedly yield new compositions of HLW, whether it be the direct fuel form or the residues from various spent fuel reprocessing strategies, that may be more compatible with alternate waste forms from either a safety, economic, or compatibility perspective. Lanthanide borosilicate (LaBS) glasses are a broad category of borosilicate glasses that often contain silica, alumina, boron oxide, and lanthanide oxides as their primary constituents, as well as various minor constituents such as barium, lead, and strontium oxide to name just a few.[24–27] These glasses are further characterized by exhibiting higher glass transition temperatures, melting temperatures, radionuclide solubility (in most cases), and chemical durability compared to traditional AAB glasses. Other favorable qualities of these glasses include the presence of significant quantities of neutron absorbers (lanthanides) that permit increased loading of fissile materials into the glass with negligible increases in the risk of criticality.[28] Due to these characteristics, LaBS glasses have been a candidate waste form for the immobilization and disposal of a wide variety of radioactive waste streams, including those containing larger quantities of fissile radionuclides,[29] salts,[30,31] and other impurities.[26,32,33] However, LaBS glasses have been substantially less studied than AAB glasses and require additional investigations to understand the effect glass composition, leachate composition, radiation, temperature, and other factors have on their forward and residual rate of dissolution.

The majority of initial studies examining the durability and properties of LaBS glasses were conducted during campaigns to immobilize waste rich in americium (Am) and curium (Cm) at the Savannah River Site to facilitate safe transport to Oak Ridge National Laboratory[26,27] or to dispose of surplus weapons-usable uranium (U) and plutonium (Pu) waste as part of the DOE's Fissile Materials Disposition Program from the mid-1990s to the mid-2000s.[32,33] In these studies, a couple hundred compositions of LaBS glasses were fabricated and tested to explore the relationship between glass composition and material durability (Product Consistency Test-A), viscosity, homogeneity, transition temperature, density, and overall solubility of various radionuclides and impurities identified in their targeted HLW feed streams. Factors important to constructing a representative source-term model for the release of radionuclides from the LaBS glass waste form, such as pH,[34,35] temperature,[35,36] saturation, radiation,[37] and leachate composition, were either assessed on only a few LaBS glass compositions, or only on AAB type glasses. Recent studies have focused on the fundamental mechanism of LaBS glass dissolution, the local environment of lanthanides within the glass by assessing simpler LaBS glass compositions, and the effect lanthanide loading has on various LaBS glass properties.[38–44] These studies are crucial for the development of representative source-term models. However, if LaBS glasses are to become a viable option for the disposal of radioactive waste, a foundational understanding of their degradation mechanism, as well as compositional-property relationships for all the aforementioned factors must be well understood. Yet, quantitative kinetic parameters for these glasses as a function of glass and leachate composition remain scarce. Establishing reliable activation energies and compositional controls over dissolution behavior provides critical data for next-generation PAMs that aim to predict the long-term evolution of these materials under coupled thermal, chemical, and radiative fields.

Here we study the effect that temperature has on the durability of AmCm2-19, a well characterized legacy LaBS glass sample from the aforementioned Am and Cm immobilization campaign, as well as Internal Simple Glass-1 (ISG-1),[45] a reference AAB glass, for comparison using the Product Consistency Test-B. These data are fit to the Arrhenius relationship to determine the activation energy of the glass's dissolution in deionized water. An AmCm2-19 glass sample leached at 200 °C for an extended period is examined for the possible presence of secondary phases or the formation of an alteration layer using powder X-ray diffraction (pXRD), scanning electron microscopy (SEM), and energy dispersive X-ray spectroscopy (EDX). No obvious secondary phases or alteration layers are observed. By extending durability testing of legacy AmCm2-19 LaBS glass to elevated temperatures, this work bridges the gap between empirical corrosion testing and parameterized modeling of complex glass degradation processes.

Results and Discussion

Temperature-Dependent Element Release Rates

The average normalized elemental release rates (NR_i) of various elements from AmCm2-19 glass and ISG-1, as determined from PCT-B accelerated leach experiments, are shown as a function of temperature from 50 °C to 250 °C in **Figure 1** and **Table S1**. Note that error bars are excluded in **Figure 1** for the sake of clarity but are shown in **Figures S1** and **S2** of the supplementary information. The values of NR_B = (1.38 ± 0.16) × 10^{-1} g m^{-2} d^{-1} and NR_{Si} = (3.11 ± 0.39) × 10^{-2} g m^{-2} d^{-1} at 100 °C for ISG-1 samples is expectedly similar to previously reported values determined from PCT-A accelerated leach testing at 90 °C.[45,48,49] This confirms the validity of the experimental setup, equipment, and accelerated leach testing procedures used in this work. For ISG-1 samples, the NR_{Si} increased with temperature from 50 °C to 250 °C, while the NR_B plateaued at temperatures ≥150 °C. For AmCm2-19 glass samples, the NR_B and NR_{Si} followed a similar trend to one another, increasing with temperature before plateauing at temperatures ≥150 °C. This behavior suggests that at temperatures ≥150 °C, the solubility limit of B and Si were reached in the leachate, and thus a secondary phase or passivating gel layer containing these elements may have formed. Interestingly, the concentrations of B (~5.5 mg L^{-1}) and Si (~13.5 mg L^{-1}) at saturation in the leachate of AmCm2-19 glass samples were about an order of magnitude lower than in the leachate of ISG-1 samples (**Figure S3** and **Table S2**). This indicates that different secondary mineral phases dictate the observed solubility of various dissolved matrix elements in the leachate of these systems. For example, Si or Al rich mineral phases, such as zeolites and silicates, may form from the leached components of AAB glasses, while lanthanide containing mineral phases, such as lanthanide silicates, lanthanide hydroxides, and strontium lanthanide oxides, may form from the leached components of LaBS glasses.[35,50,51]

Lanthanide Release Trends and Network-Structure Effects

The NR_i of all measured lanthanides, with the exception of Ce, from AmCm2-19 glass samples decreased with increasing atomic number (**Figure 1**). When trivalent lanthanides are incorporated into glass, they often act as network-modifying species,[39,40,52,53] although they have also been reported to behave as intermediate oxides under some conditions,[54] that interrupt the formation of bridging oxygen bonds between network-forming species (i.e., SiO_2 and B_2O_3). This results in the formation of non-bridging oxygen groups that interact with the lanthanides in the disrupted amorphous network of the glass.[40,55] Due to the ionic nature of these interactions, the more charge dense (harder) late lanthanides, compared to the less charge dense (softer) early lanthanides, form stronger interactions with the hard non-bridging oxygen donors of the network. This is likely the reason why early lanthanides are more rapidly leached from AmCm2-19 glass samples than the late lanthanides. This behavior remained prevalent across the temperature range of 50 °C to 250 °C.

The NR_{Ce} from AmCm2-19 glass samples did not follow the trend observed with other lanthanides. This may be due to a few characteristics of Ce compared to the other lanthanides assessed here. Ce may exist in either the tri- or tetra-valent state within the glass and throughout the leaching process, while the other lanthanides are redox-inactive and remain trivalent. The increased charge and smaller ionic radius of Ce(IV) could result in a stronger interaction with the non-bonding oxygens of the glass network. However, it is unlikely that there is Ce(IV) present in the AmCm2-19 glass utilized in this work, as the fabrication process utilized to make this legacy sample favored the complete reduction of Ce(IV) to Ce(III).[56] Regardless, Ce has been reported to behave as an intermediate in glass networks, functioning as both a network modifier and network former,[57,58] likely leading to the varied behavior observed here.

Activation Energies and Kinetic Control of Glass Degradation

The goal of the temperature dependence study was to determine the activation energy of the rate-limiting reaction governing the degradation of AmCm2-19 glass in the early phase of alteration in deionized water. The concentration of B and Si in the leachate (**Table S2**) plateaued at temperatures ≥ 150 °C (~5.5 mg L^{-1} for B, and ~13.5 mg L^{-1} for Si), likely corresponding to the solubility limit of a secondary mineral phase, so these data were not utilized for the calculation of Arrhenius parameters related to the alteration of the AmCm2-19 glass. **Figure 2** shows the measured NR_i data fit to the Arrhenius relationship:

$$NR_i = Ae^{-\frac{E_a}{RT}} \quad \textbf{(3)}$$

where A is the preexponential coefficient and E_a is the activation energy. The data collected at 50 °C and 100 °C were used to calculate activation energy values of E_a(B) = 24.8 ± 0.3 kJ mol^{-1} and E_a(Si) = 14.4 ± 0.2 kJ mol^{-1}. These values, along with literature values for other tested compositions of LaBS glasses, are listed in **Table 1**. The E_a of AmCm2-19 glass dissolution was lower than that of Pu-LaBS-B glass[35] and within the range of values calculated (see SI for details) for Am/Cm Target glass.[36] Notably, the range of activation energies for LaBS glasses range from *ca*. 10-50 kJ mol^{-1} while those for AAB glasses range from *ca*. 60-90 kJ mol^{-1}.[12] This observation emphasizes a stark difference between these two classes of glasses. The composition-dependent difference in E_a between these LaBS glasses highlights the need to build a library of intrinsic glass durability parameters versus LaBS glass composition to facilitate their implementation into PAMs. Additionally, other accelerated leaching methods that maintain dilute conditions, such as single-pass flow through experiments, should be conducted with AmCm2-19 glass to verify that the value of E_a determined here corresponds to the rate-limiting reaction of the forward rate regime.

While the AmCm2-19 glass samples did not show notable visual signs of alteration or secondary phase formation from 50 °C to 250 °C, ISG-1 samples exhibited signs of alteration under all tested conditions, forming large granules at 50 °C and 100 °C, and fused materials at temperatures above 150 °C (**Figure S4**). The shift in ISG-1 sample morphology throughout the leaching study likely decreased the reactive surface area of the sample over time, especially at elevated temperatures, increasing the uncertainty of the calculation of NR_B and NR_{Si}. If the initial surface area of the sample is assumed constant over the duration of the study, calculated values of NR_i would be lower, proportional to the ratio of assumed surface area to actual surface area. Thus, these NR_i values provide a bound for the minimum degradation rate of the material. With the assumption that the surface areas of ISG-1 samples are equal to their initial values over the duration of the study, and that a single rate-limiting reaction governed the measured NR_B and NR_{Si} across the entire temperature range, the data were fit to the Arrhenius relationship to give activation energy values of E_a(B) = 9.2 ± 0.7 kJ mol^{-1} and E_a(Si) = 10.5 ± 0.6 kJ mol^{-1}, respectively. These values are significantly lower than those previously determined from forward rate measurements of ISG-1 and ISG-0 dissolution, which range from *ca*. 60-80 kJ mol^{-1}.[59,60] Although these activation energies should not be used directly due to questions regarding the change in surface area of the sample over time and affinity affects, the measured C_i values (**Figure S3** and **Table S2**) may be valuable data for comparison in future studies.

Characterization of Structural Integrity upon Leaching

To assess the potential formation of an alteration layer or secondary mineral phase, a higher surface area AmCm2-19 glass sample (-200 mesh; ≲ 75 μm) with fines was leached at 200 ± 1 °C for 16.826 days in a PTFE vessel to facilitate reaching saturated conditions in the leachate. The resulting AmCm2-19 glass sample was isolated from the leachate and dried at 50 °C overnight. pXRD patterns of AmCm2-19 glass before and after leaching are shown in **Figure 3**. The spectrum of pristine AmCm2-19 glass has a broad feature centered at approximately 32° 2θ and a minor but sharp feature at approximately 40° 2θ. The broad feature is characteristic of the amorphous glass matrix, while the sharp feature likely corresponds to the inclusion of a small quantity of a crystalline rare earth silicate phase generated during the fabrication of the material.[26,46] After leaching, the broad feature at approximately 32° 2θ remained unchanged while the sharp feature at approximately 40° 2θ decreased in intensity. It is unclear whether this is due to the selective dissolution of the crystalline rare earth silicate phase during leaching or to the formation of an amorphous alteration layer that attenuates the X-ray beam prior to reaching the underlying crystalline phase, reducing the observed signal. Additionally, these spectra indicate that a secondary crystalline phase was not formed in detectable quantities from the leaching experiment.

SEM secondary electron images of the pristine and leached -200 mesh AmCm2-19 glass samples are shown in **Figure 4**. Both pristine and leached samples show striations, which are characteristic of the fracturing of the material during the crushing procedure. The quantity and size of adhered fines slightly decreased due to their dissolution. No obvious secondary phase or surface alteration were observed in images of the leached AmCm2-19 sample. A semi-quantitative elemental analysis of the surface of representative particles from pristine and leached AmCm2-19 glass samples was performed using EDX (**Figure 5**, **Figure S5** and **Table S3**). Negligible changes in surface composition was observed

between the samples. These images and semi-quantitative elemental analysis data suggest that an alteration layer was likely not present on the surface of these samples or was too thin to observe and measure using SEM and EDX, respectively. Longer term leaching trials are underway to form and analyze secondary phases or alteration layers in these samples but are beyond the scope of this analysis and will be discussed in subsequent reports.

The effect temperature has on the dissolution rate of AmCm2-19 glass and ISG-1 were assessed from 50 °C to 250 °C in deionized water using the PCT-B protocol. For AmCm2-19 samples, the concentration of B and Si in the leachate plateaued at temperatures ≥ 150 °C. Thus, only data at 50 °C and 100 °C were used to calculate the activation energy of AmCm2-19 glass dissolution in deionized water of E_a(B) = 24.8 ± 0.3 kJ mol^{-1} and E_a(Si) = 14.4 ± 0.2 kJ mol^{-1}. The leached ISG-1 samples were notably altered, such that the reactive surface area of the samples over the course of the study were likely significantly different leading to large uncertainty in calculated NR_i and E_a values. The calculated activation energy of ISG-1 dissolution in deionized water of E_a(B) = 9.2 ± 0.7 kJ mol^{-1} and E_a(Si) = 10.5 ± 0.6 kJ mol^{-1} are significantly lower than those calculated using forward rate measurements in other studies. From SEM imaging, EDX elemental analysis, and pXRD measurements, no obvious secondary phases or alteration layers were observed on AmCm2-19 glass samples leached under the conditions studied here. Extended static-leaching experiments are underway to generate and characterize these elusive phases. To the best of the authors' knowledge, the activation energy of AmCm2-19 glass dissolution reported in this work represents that of the third such LaBS glass composition in the literature. While these findings expand the quantitative foundation for modeling temperature-dependent LaBS glass corrosion, similar studies of significantly more LaBS glass compositions are needed to identify composition-activation energy relationships that may inform the selection of parameters in the performance assessment modeling of these waste forms in deep geological repositories.

Methods

Materials

Samples of International Simple Glass-1 (ISG-1) and AmCm2-19 (LaBS) glass were obtained from Pacific Northwest National Laboratory (PNNL). The AmCm2-19 glass was a legacy sample from a previous study published in 2019.[46] Their composition is shown in **Table 2**. Optima grade 67-70 wt.% nitric acid (HNO_3), extra pure 50 wt.% sodium hydroxide (NaOH), ASTM type 1 water, 200 proof absolute ethanol, 50 ppm rare earth element ICP standard in 2 wt.% HNO_3, individual 1000 ppm Si, Al, B, and In (indium) ICP standards in 2 wt.% HNO_3, and sterilized, metal free polypropylene 15 mL centrifuge tubes were purchased from chemical retailers (Thermo Fisher Scientific and VWR) and used as received. Reaction vessels were purchased from Parr Instrument Company and consisted of a 4749 General Purpose Acid Digestion Vessel paired with an A280AC 23 mL PTFE (polytetrafluoroethylene) Cup and Cover. All heating processes were conducted using a Binder (Model FP56-UL) oven, manufactured with a thermocouple and datalogger. Oven temperatures were recorded in 30-minute increments over the duration of an experiment and were constant within 1 °C of the set point. Fluoride ion and pH measurements were conducted using a Thermo Scientific Orion STAR A214 pH/ISE meter with a Thermo Scientific Orion Fluoride Ionplus Sure Flow electrode (9609BNWP) or Thermo Scientific ORION Ross Ultra Triode pH electrode (8302BNUMD), respectively. Measured potentials were compared against 3-point calibration curves made with calibration standards. The average error of pH measurements over the duration of the study was ± 0.05. The balance (VWR-310AC) was checked for accuracy prior to weighing samples and vessels using ISO/IEC 17025 certified calibration weights (Troemner). The average error of mass measurements over the duration of the study was ± 0.0002 g.

Sample Preparation for Accelerated Leach Testing

ISG-1 and AmCm2-19 samples were crushed using a tungsten carbide puck mill (SPEX Shatterbox). Crushed samples were mechanically sieved (W.S. Tyler; ASTM E11 Standard) to obtain the +200/-100 mesh (75–150 µm) and the -200 mesh (<75 µm) size fractions. Sieved samples were cleaned of fines following the ASTM C1285.21 protocol.[47] The absence of fines and other potential contamination (e.g., tungsten carbide from the disc mill) was verified using scanning electron microscopy (JEOL JSM IT800HL) in secondary electron and backscattered electron detection modes.

Vessel Preparation for Accelerated Leach Testing

PTFE vessels were cleaned according to the ASTM C1285.21 protocol.[47] Briefly, new vessels were rinsed with ASTM type 1 water, filled >90% with 5 wt.% NaOH, sealed, and heated at 110 ± 1 °C for >7 days. Once removed from the oven and cooled, the vessels were emptied, rinsed with ASTM type 1 water, and then boiled in ASTM type 1 water for >1 hour. This was repeated two more times. The vessels were then filled >90% with ASTM type 1 water, sealed, and heated at 90 ± 1 °C for >16 hours. Once removed from the oven and cooled, aliquots of the water were used to test for pH and fluoride ion content. The vessels were considered clean when the measured pH was between 5-7 and fluoride ion concentration was <0.5 µg/mL. If they did not meet these requirements, all the steps following the 5 wt.% NaOH leach were repeated. Used vessels were subjected to a similar series of cleaning and testing steps, with the exception that the 5 wt.% NaOH leaching step was replaced with boiling the vessel in 1 wt.% HNO_3 for >1 hour to ensure any leftover samples were removed from the vessel.

Accelerated Leach Testing

Accelerated leach testing was conducted in accordance with the Product Consistency Test-B (PCT-B) from the ASTM C1285.21 protocol.[47] This involved heating PTFE pressure vessels filled with either ASTM Type 1 water (blanks), ISG-1 and ASTM Type 1 water (references), or AmCm2-19 and ASTM Type 1 water (samples) at temperatures of 50, 100, 150, 200, and 250 °C for a duration of 7 ± 0.14 days, after which the blanks, references, and samples were cooled to room temperature and prepared for elemental analysis (see the following section). Blanks, references, and samples were prepared and tested in triplicate at each temperature point. For ISG-1 samples, the SA/V was held at 2130.8 ± 8.8 m^{-1}. For AmCm2-19 samples, the SA/V was held at 1288.9 ± 4.2 m^{-1}. The SA of ISG-1 and AmCm2-19 samples were estimated from their mass and density by assuming the average particle was spherical with a diameter of 112.5 µm. The density of ISG-1 used here was 2.508 g/cm^3.[45] The density of AmCm2-19 was reported to be 4.0342 g/cm^3 from buoyancy measurements and 4.263 g/cm^3 from gas pycnometry measurements.[26] The average value of 4.1486 g/cm^3 was used here. All experimental parameters for each blank, reference, and sample are listed in **Table S4** of the supplemental information.

Inductively Couple Plasma – Optical Emission Spectroscopy (ICP-OES) Sample Preparation and Measurements

Elemental analysis was performed using a PerkinElmer Avio 500 ICP-OES paired with a PerkinElmer S23 Autosampler. Samples were prepared as follows. An aliquot of the blank or sample's leachate was filtered through a 0.45 µm hydrophilic PTFE syringe filter (VWR) and then acidified to 2 wt.% HNO_3 using optima grade HNO_3. This mixture was spiked with 10 ppm In as an internal reference to correct for instrument drift and minor matrix effects. When necessary, samples were further diluted with a stock of 2 wt.% HNO_3 containing 10 ppm In to ensure measurements were within the range of the calibration curve. Calibration solutions of nominally 0.01, 0.05, 0.1, 0.5, 1.0, 2.0, 4.0, 6.0, 8.0, and 10.0 ppm were prepared from ICP standards of B, Al, Si, La, Ce, Pr, Nd, Sm, Eu, Eu, Gd, and Er and spiked with 10 ppm In as an internal reference. Nitrogen was used as a sheer gas and the plasma was aligned in an axial view using a 1 ppm Mn stock solution. The risk of sample crossover was minimized by washing the system with 2 wt.% HNO_3 for 30 seconds between samples. Nine spectra were acquired and averaged per sample. If the signal of the internal reference deviated by >20%, the data was not accepted.

Data Analysis

Measured intensities for individual blanks were averaged and corrected using the internal In reference. Corrected measurements from the triplicate sample blanks (PTFE vessels filled with the leachate but no sample) were averaged together and the standard deviation between these samples was determined. The limit of quantification (LOQ) was determined by adding 10 standard deviations to the average sample blank measurement. If a sample measurement was below the LOQ, it was not included in the calculation of normalized rates. Sample data was processed according to the ASTM C1285.21 protocol.[47] For ISG-1 and AmCm2-19 samples, measured intensities for individual samples were averaged and corrected using the internal In reference and then background corrected using the blank. The corrected intensities were converted to concentrations using calibration curves and then corrected for evaporative loss by multiplying by the solution's volume ratio ($V_{final}/V_{initial}$). In all cases the maximum loss of leachate volume from evaporation was less than 0.5 %. This corrected concentration for each element (C_i) was then normalized to account for the mass fraction of element "i" in the glass sample (f_i). The normalized concentration of each element (NC_i) was

then converted into a normalized elemental leach rate (NR_i) by accounting for the SA/V ratio and duration of the experiment. Normalized elemental leach rates from triplicate samples were averaged and the standard deviation between samples was determined. The average normalized leach rates for B and Si at each temperature point was used to calculate the activation energy of ISG-1 and AmCm2-19 dissolution in deionized water by performing a linear fit of data plotted as $\ln(NR_i)$ vs. 1,000/T, where T is the temperature in units of K and NR_i is in units of g m^{-2} d^{-1}.

Sample Preparation to Promote Secondary Phase/Alteration Layer Formation

A 1.2596 ± 0.0002 g -200 mesh (<75 µm) AmCm2-19 sample that contained fines was leached in 3.1765 ± 0.0002 g of ASTM type 1 water (SA/V > 7633 m^{-1}) at 200 °C for 16.826 days to favor the formation of an alteration layer or secondary phase. The leached AmCm2-19 glass sample was removed from the leachate without rinsing and dried at 50 °C overnight. The dried sample was assessed using SEM imaging (JEOL JSM IT800HL), EDX (JEOL JSM IT800HL), and pXRD (Rigaku XtaLAB Synergy-S diffractometer).

Powder X-ray Diffraction

Samples were loaded onto a MiTeGen loop using silicon grease and mounted in a Rigaku XtaLAB Synergy-S diffractometer equipped with a PhotonJet X-ray source (Cu Kα radiation, λ = 1.5406 Å) and HyPix-6000HE detector. Samples were cooled to 100 K and diffraction data was collected in "powder pattern" mode using an exposure time of 1200 s for all theta positions.

Scanning Electron Microscopy (SEM) and Energy Dispersive X-ray Spectroscopy (EDX)

Samples were adhered to conductive carbon tape and coated with 17 nm of carbon using an ACE600 Leica carbon coater to mitigate sample charging. The samples were loaded into a JEOL JSM IT800HL SEM equipped with an In lens Schottky plus field emission electron gun (operating at an accelerating voltage of 20 kV) and an Oxford Instruments Ultim Max 100 mm^2 127eV Energy Dispersive Spectrometer. All SEM images and EDX measurements were collected under high vacuum. The EDX measurements collected here are semi-quantitative and should only be used for the comparison of samples reported in this work.

Data Availability

All data are available in the manuscript and supplementary information file or can be obtained from the corresponding authors upon request.

Acknowledgments

The authors thank Dr. Brian Riley, Dr. Vivianaluxa Gervasio, Dr. Benjamin Parruzot, and Dr. Joelle Reiser of the Radiological Materials group at PNNL for fruitful discussion and for providing samples of ISG-1 and AmCm2-19 glass. The authors thank John Grimsich from the Department of Earth and Planetary Sciences at UC Berkeley for his guidance with SEM imaging and EDX measurements.

Funding Declaration

This work was supported by the Advanced Research Projects Agency - Energy (ARPA-E) of the U.S. Department of Energy (DOE; ARPA-E Grant No. DE-AR0001621); part of the research was conducted at the Lawrence Berkeley National Laboratory, a U.S. DOE Office of Science national laboratory managed by the University of California (UC) under contract No. DE-AC02-05CH11231.

Author Contributions

JRM – Conceptualization (equal); formal analysis; investigation; methodology (lead); project administration; supervision; visualization; data curation; writing – original draft.
DAS – Investigation; methodology (supporting); writing – review and editing.

JAG – Investigation; methodology (supporting).
TW – Investigation; methodology (supporting).
LGC – Investigation.
EB – Conceptualization (equal); writing – review and editing.
SF – Conceptualization (equal); writing – review and editing.
JS – Conceptualization (equal); funding acquisition (equal); writing – review and editing.
RS – Conceptualization (equal); funding acquisition (equal); writing – review and editing.
PFP – Conceptualization (equal); funding acquisition (equal); supervision; writing – review and editing.
RJA - Conceptualization (equal); funding acquisition (equal); resources; supervision; writing – review and editing.

Competing Interests

PFP declares financial interest in Deep Isolation Nuclear, Inc, and both he and the company could benefit from commercialization of products, the development of which is supported by this research. All other authors declare no competing financial or non-financial interests.

References

1. INTERNATIONAL ATOMIC ENERGY AGENCY, Roadmap for Implementing a Geological Disposal Programme. Report No. NW-T-1.43. (2024).
2. King, F. et al. Review of the Modelling of Corrosion Processes and Lifetime Prediction for HLW/SF Containers—Part 2: Performance Assessment Models. Corrosion and Materials Degradation **5**, 289–339 (2024).
3. Ruiz-Fresneda, M. A. et al. Impact of microbial processes on the safety of deep geological repositories for radioactive waste. Front. Microbiol. **14**, (2023).
4. Morales-Hidalgo, M. et al. Insights into the Impact of Physicochemical and Microbiological Parameters on the Safety Performance of Deep Geological Repositories. Microorganisms **12**, 1025 (2024).
5. Andrews, N. C. et al. Mechanistic Source Term Considerations for Advanced Non-LWRs. Report No. SAND2021-2668. (2021).
6. Jantzen, C. M. & Ojovan, M. I. On Selection of Matrix (Wasteform) Material for Higher Activity Nuclear Waste Immobilization (Review). Russ. J. Inorg. Chem. **64**, 1611–1624 (2019).
7. Thorpe, C. L. et al. Forty years of durability assessment of nuclear waste glass by standard methods. npj Mater Degrad **5**, 61 (2021).
8. Frankel, G. S. et al. Recent Advances in Corrosion Science Applicable To Disposal of High-Level Nuclear Waste. Chem. Rev. **121**, 12327–12383 (2021).
9. Gin, S., Jollivet, P., Tribet, M., Peuget, S. & Schuller, S. Radionuclides containment in nuclear glasses: an overview. Radiochimica Acta **105**, 927–959 (2017).
10. Gin, S. et al. Insights into the mechanisms controlling the residual corrosion rate of borosilicate glasses. npj Mater Degrad **4**, 41 (2020).
11. Fournier, M., Gin, S. & Frugier, P. Resumption of nuclear glass alteration: State of the art. Journal of Nuclear Materials **448**, 348–363 (2014).
12. Vienna, J. D., Neeway, J. J., Ryan, J. V. & Kerisit, S. N. Impacts of glass composition, pH, and temperature on glass forward dissolution rate. npj Mater Degrad **2**, 22 (2018).
13. Grambow, B. A General Rate Equation for Nuclear Waste Glass Corrosion. MRS Online Proceedings Library (OPL) **44**, 15 (1984).
14. Oelkers, E. H. General kinetic description of multioxide silicate mineral and glass dissolution. Geochimica et Cosmochimica Acta **65**, 3703–3719 (2001).
15. Frugier, P. et al. SON68 nuclear glass dissolution kinetics: Current state of knowledge and basis of the new GRAAL model. Journal of Nuclear Materials **380**, 8–21 (2008).
16. Frugier, P., Minet, Y., Rajmohan, N., Godon, N. & Gin, S. Modeling glass corrosion with GRAAL. npj Mater Degrad **2**, 35 (2018).

17. Minet, Y., Bonin, B., Gin, S. & Frugier, P. Analytic implementation of the GRAAL model: Application to a R7T7-type glass package in a geological disposal environment. Journal of Nuclear Materials **404**, 178–202 (2010).
18. Delcroix, M., Frugier, P., Geiger, E. & Noiriel, C. The GRAAL2 glass alteration model: initial qualification on a simple chemical system. npj Mater Degrad **9**, 38 (2025).
19. Strachan, D. Defense HLW Glass Degradation Model. Report No. ANL-EBS-MD-000016. (2004).
20. Yucca Mountain Repository License Application Safety Analysis Report. Report No. DOE/RW-0573. (2008).
21. Curti, E. Aqueous Corrosion of Vitrified Nuclear Waste: Current Process Understanding, Literature Review and Recommended Rates. Report No. NAB 23-09. (2022).
22. Kelly, J. E. Generation IV International Forum: A decade of progress through international cooperation. Progress in Nuclear Energy **77**, 240–246 (2014).
23. Generation IV Nuclear Reactors - World Nuclear Association. https://world-nuclear.org/information-library/nuclear-fuel-cycle/nuclear-power-reactors/generation-iv-nuclear-reactors.
24. Bibler, N. E., Ramsey, W. G., Meaker, T. F. & Pareizs, J. M. Durabilities and Microstructures of Radioactive Glasses for Immobilization of Excess Actinides at the Savannah River Site. MRS Online Proceedings Library (OPL) **412**, 65 (1995).
25. Crawford, C. L., Marra, J. C. & Bibler, N. E. Glass fabrication and product consistency testing of lanthanide borosilicate glass for plutonium disposition. Journal of Alloys and Compounds **444–445**, 569–579 (2007).
26. Peeler, D. Composition/Property Relationship for the Phase 2 Am-Cm Glass Variability Study. Report No. WSRC-TR-99-00393. (2000).
27. Peeler, D. K. et al. Composition/Property Relationships for the Phase 1 Am/Cm Glass Variability Study. Report No. WSRC-TR-99-00055. (1999).
28. Marra, J. C., Peeler, D. K. & Jantzen, C. M. Development of an Alternative Glass Formulation for Vitrification of Excess Plutonium. Report No. WSRC-TR-2006-00031. (2006).
29. Peeler, D. K. et al. Results of an Inter-Laboratory Study of Glass Formulation for the Immobilization of Excess Plutonium. Report No. SRT-PUM-97-0017. (1997).
30. Riley, B. J. Electrochemical Salt Wasteform Development: A Review of Salt Treatment and Immobilization Options. Ind. Eng. Chem. Res. **59**, 9760–9774 (2020).
31. Riley, B. J. & Chong, S. Glass waste form options for rare-earth fission products from electrochemical reprocessing. Journal of Non-Crystalline Solids **545**, 120161 (2020).
32. Fox, K. M., Marra, J. C., Edwards, T. B., Hoffman, E. N. & Crawford, C. L. Plutonium Feed Impurity Testing in Lanthanide Borosilicate (LaBS) Glass. MRS Online Proceedings Library (OPL) **1107**, 397 (2008).
33. Fox, K. M. et al. Variability Study to Determine the Solubility of Impurities in Plutonium-Bearing, Lanthanide Borosilicate Glass. Report No. WSRC-STI-2007-00477. (2007).
34. Daniel, W. E. & Best, D. R. Am/Cm Target Glass Durability Dependence on pH (U). Report No. WSRC-MS-96-0165. (1996).
35. Ebert, W. L. Corrosion Testing of a Plutonium-Loaded Lanthanide Borosilicate Glass Made with Frit B. Report No. ANL-06/35. (2006).
36. Daniel, W. E. & Best, D. R. Time, Temperature, and Compositional Study of Am/Cm Target Glass Durability. Report No. WSRC-MS-96-0163. (1996).
37. Deschanels, X., Peuget, S., Cachia, J. N. & Charpentier, T. Plutonium solubility and self-irradiation effects in borosilicate glass. Progress in Nuclear Energy **49**, 623–634 (2007).
38. Fabian, M., Pinakidou, F., Tolnai, I., Czompoly, O. & Osan, J. Lanthanide (Ce, Nd, Eu) environments and leaching behavior in borosilicate glasses. Sci Rep **11**, 13272 (2021).
39. Fabian, M. et al. Structural investigation of borosilicate glasses containing lanthanide ions. Sci Rep **10**, 7835 (2020).
40. Tolnai, I. et al. Structural characterization of uranium and lanthanide loaded borosilicate glass matrix. Sci Rep **15**, 28352 (2025).
41. Mabrouk, A., Vaills, Y., Pellerin, N. & Bachar, A. Structural study of lanthanum sodium aluminoborosilicate glasses by NMR spectroscopy. Materials Chemistry and Physics **254**, 123492 (2020).
42. Kim, M., Ha, M. G., Um, W., Kim, H. G. & Hong, K.-S. Relationship between leaching behavior and glass structure of calcium-aluminoborate waste glasses with various La_2O_3 contents. Journal of Nuclear Materials **539**, 152331 (2020).
43. Malchukova, E., Levitskii, V., Tyurnina, N. & Tyurnina, Z. Structure and optical behavior of mixed lanthanides aluminoborosilicate glasses. Ceramics International **51**, 9570–9576 (2025).

44. Nicoleau, E. et al. Rare-earth silicate crystallization in borosilicate glasses: Effect on structural and chemical durability properties. Journal of Non-Crystalline Solids **438**, 37–48 (2016).
45. Ryan, J. V. et al. ISG-2: properties of the second International Simple Glass. npj Mater Degrad **7**, 47 (2023).
46. Gervasio, V. et al. Liquidus Temperature: Assessing Standard Glasses for Furnace Calibration. Report No. PNNL-29312. (2019).
47. Standard Test Methods for Determining Chemical Durability of Nuclear, Hazardous, and Mixed Waste Glasses and Multiphase Glass Ceramics: The Product Consistency Test (PCT). Report No. ASTM C1285-21. (2021).
48. Jiménez, J. A., Crawford, C. L., Lascola, R. J., Christian, J. H. & Foley, B. J. Physico-chemical properties of γ-irradiated International Simple Glass (ISG) nuclear waste simulants with low levels of iron impurities. Chemical Physics Impact **6**, 100233 (2023).
49. Jiménez, J. A., Crawford, C. L. & Lascola, R. J. Physico-chemical properties of international simple glass (ISG) nuclear waste simulants: Luminescence baseline study. Journal of the American Ceramic Society **105**, 4009–4026 (2022).
50. Li, L., Strachan, D. M., Li, H., Davis, L. L. & Qian, M. Crystallization of gadolinium- and lanthanum-containing phases from sodium alumino-borosilicate glasses. Journal of Non-Crystalline Solids **272**, 46–56 (2000).
51. Fortner, J. A., Mertz, C. J., Chamberlain, D. C. & Bates, J. K. Plutonium Alteration Phases from Lanthanide Borosilicate Glass. Report No. ANL/CMT/CP--92880. (1997).
52. Gaddam, A., Fernandes, H. R., Tulyaganov, D. U. & Ferreira, J. M. F. The structural role of lanthanum oxide in silicate glasses. Journal of Non-Crystalline Solids **505**, 18–27 (2019).
53. Hordieiev, Yu. S. & Zaichuk, A. V. Study of the Influence of R2O3 (R = Al, La, Y) on the Structure, Thermal and some Physical Properties of Magnesium Borosilicate Glasses. J Inorg Organomet Polym **33**, 591–598 (2023).
54. Angeli, F. et al. Influence of lanthanum on borosilicate glass structure: A multinuclear MAS and MQMAS NMR investigation. Journal of Non-Crystalline Solids **376**, 189–198 (2013).
55. Molières, E. et al. Chemical Durability of Lanthanum-Enriched Borosilicate Glass. International Journal of Applied Glass Science **4**, 383–394 (2013).
56. Peeler, D. K., Marra, J. E., Reamer, I. A., Vienna, J. D. & Li, H. Development of the Am/Cm Batch Vitrification Process. Report No. WRSC-MS-99-00657. (1999).
57. Deshpande, V. K. & Taikar, R. N. Effect of cerium oxide addition on electrical and physical properties of alkali borosilicate glasses. Materials Science and Engineering: B **172**, 6–8 (2010).
58. Mekki, A. X-ray photoelectron spectroscopy of CeO2–Na2O–SiO2 glasses. Journal of Electron Spectroscopy and Related Phenomena **142**, 75–81 (2005).
59. Inagaki, Y., Kikunaga, T., Idemitsu, K. & Arima, T. Initial Dissolution Rate of the International Simple Glass as a Function of pH and Temperature Measured Using Microchannel Flow-Through Test Method. International Journal of Applied Glass Science **4**, 317–327 (2013).
60. Neeway, J. J., Rieke, P. C., Parruzot, B. P., Ryan, J. V. & Asmussen, R. M. The dissolution behavior of borosilicate glasses in far-from equilibrium conditions. Geochimica et Cosmochimica Acta **226**, 132–148 (2018).

Figures and Tables

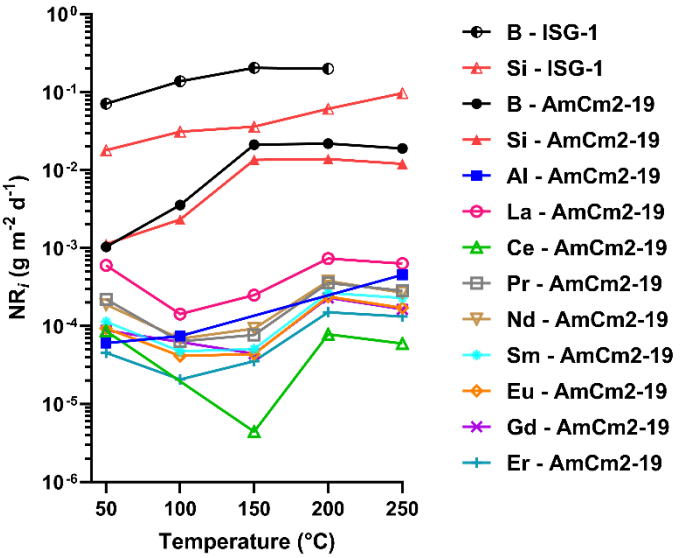

Figure 1. A plot of average measured NR_i values for various elements verses leaching temperature for ISG-1 and AmCm2-19 glass samples. Error bars have been excluded from the figure for clarity. **Figure S1** and **S2** display these data with error bars but separated into several figures. A tabulated form of these data is available in **Table S1.**

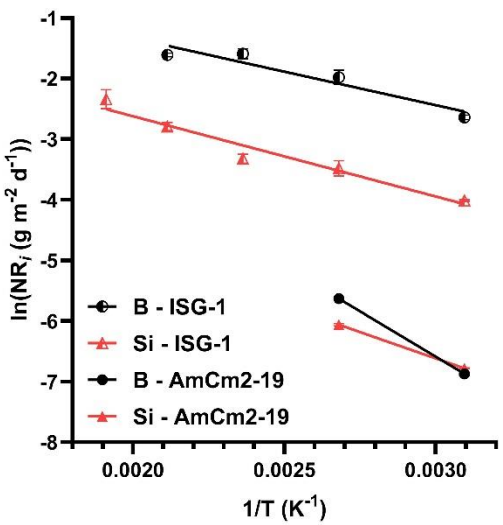

Figure 2. Arrhenius plot of NR_B (**circles**) and NR_{Si} (**triangles**) from ISG-1 and AmCm2-19 glass samples. Error bars represent one standard deviation from sample triplicate measurements. Plotted data are listed in **Table S1** and calculated activation energies of AmCm2-19 dissolution are listed in **Table 1**.

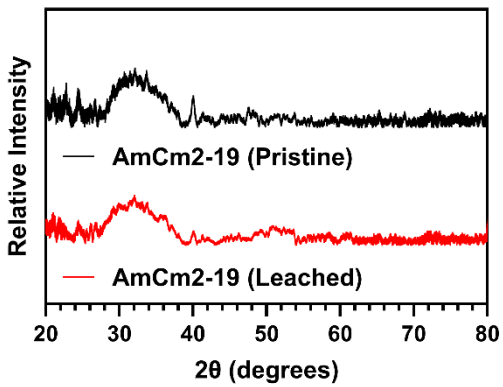

Figure 3. pXRD patterns of pristine (**black**) and leached (**red**) AmCm2-19 glass samples.

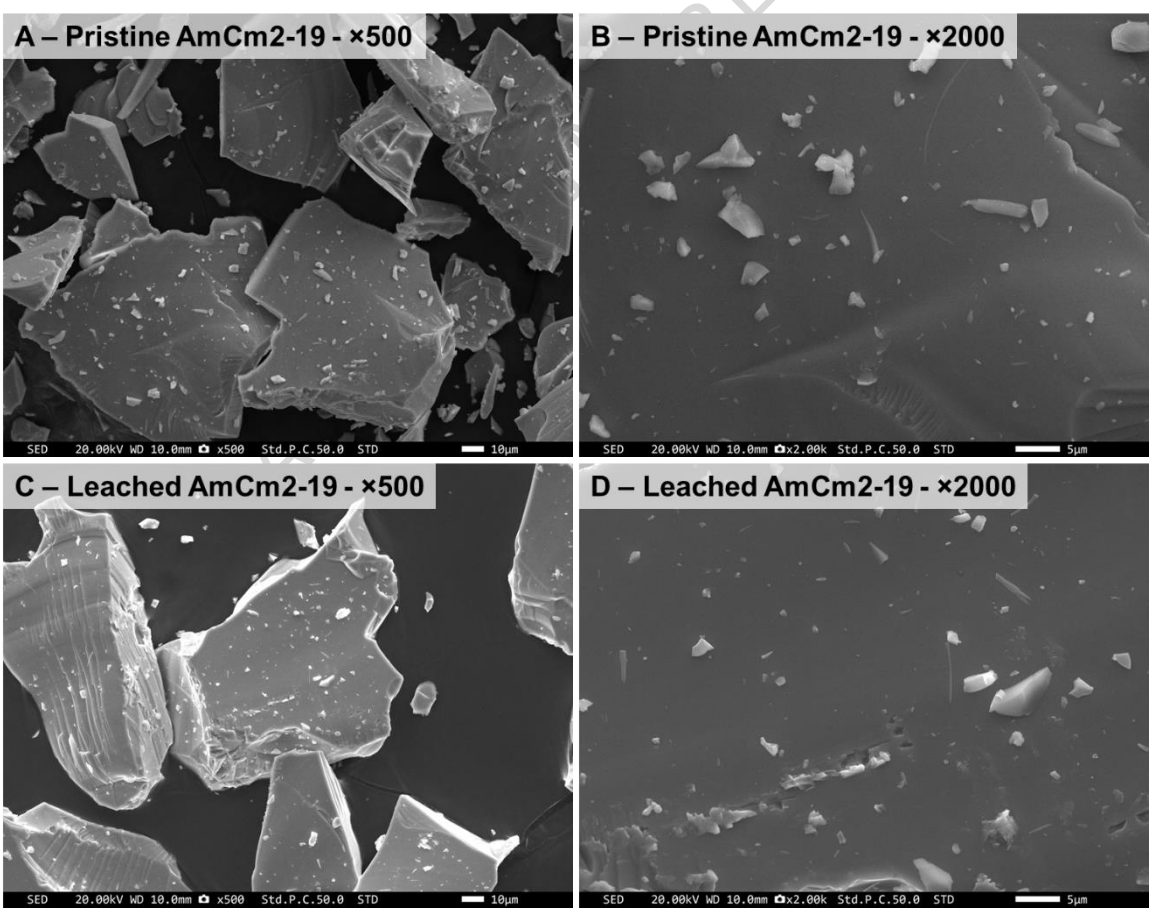

Figure 4. Secondary electron – scanning electron microscopy images of (**A** and **B**) pristine AmCm2-19 glass and (**C** and **D**) leached AmCm2-19 glass samples at (**A** and **C**) ×500 and (**B** and **D**) ×2000 magnification.

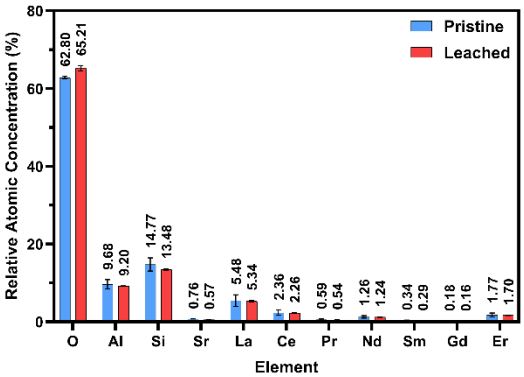

Figure 5. Average relative atomic concentrations of the surface/near surface of pristine (**blue**) and leached (**red**) AmCm2-19 glass samples measured using EDX. Error bars represent the standard deviation of 5 measurements made at various areas on a representative particle (**Figure S5**). Note that these values are semi-quantitative and should only be used for the comparison of samples reported in this work.

Table 1. Activation energy of various compositions of LaBS glasses. All values of activation energy are reported in units of kJ mol^{-1}.

Glass	pH Regime	E_a(B)	d(E_a(B))	E_a(Si)	d(E_a(Si))	Reference
Pu-LaBS-B	Acidic	48.9	-	40.5	-	[35]
Pu-LaBS-B	Alkaline	51.2	-	25.0	-	[35]
Am/Cm Target – 1-Day Leach*	Acidic/Near Neutral	19.5	3.5	22.1	1.2	[36]
Am/Cm Target – 3-Day Leach*	Acidic/Near Neutral	29.6	6.1	19.5	2.8	[36]
Am/Cm Target – 5-Day Leach*	Acidic/Near Neutral	9.9	3.1	24.6	3.2	[36]
Am/Cm Target – 7-Day Leach*	Acidic/Near Neutral	17.3	1.3	17.1	1.3	[36]
AmCm2-19	Acidic/Near Neutral	24.8	0.3	14.4	0.2	This Work

*E_a values determined from fitting reported data to the Arrhenius equation – see Supplemental Information for additional details.

Table 2. Composition of ISG-1 and AmCm2-19 glasses.

Component	**AmCm2-19 (wt.%)**[46]	**ISG-1 (wt.%)**[45]
Al_2O_3	11.90	6.00
B_2O_3	9.20	17.30
CaO	-	4.90
Ce_2O_3	9.80	-
Er_2O_3	9.10	-
Eu_2O_3	0.30	-
Gd_2O_3	1.00	-
La_2O_3	22.20	0.15
Na_2O	-	12.00
Nd_2O_3	6.00	-
Pr_2O_3	2.60	-
SiO_2	23.40	56.30
Sm_2O_3	1.50	-
SrO	2.00	-
ZrO_2	-	3.30